Prediction of the surface temperature of building-integrated photovoltaics: development of a high accuracy correlation using Computational Fluid Dynamics

Ruijun Zhang[1], Parham A. Mirzaei[1*], Jan Carmeliet[2,3]

[1]*Architecture and Built Environment Department, The University of Nottingham, Nottingham NG7 2RD, UK*
[2]*Laboratory for Building Science and Technology, Swiss Federal Laboratories for Materials Testing and Research (Empa), Uberlandstrasse 129, 8600 Dubendorf, Switzerland*
[3]*Swiss Federal Institute of Technology Zurich (ETHZ), Wolfgang-Pauli-Strasse 15, 8093 Zurich, Switzerland*

**Corresponding author: parham.mirzaei_ahranjani@nottingham.ac.uk*

Abstract

Building-integrated photovoltaic (BIPV) panels are generally expected to operate for over 25 years to be viewed as an economically viable technology. Overheating is known to be one of the major deficiencies in reaching the targeted lifespan goals. Alongside the thermal degradation, the operational efficiency of the silicon-based solar panel drops when the surface temperature exceeds certain thresholds close to 25℃. Wind-driven cooling, therefore, is widely recommended to decrease the surface temperature of PV panels using cavity cooling through their rear surfaces. Wind-driven flow can predominantly contribute to cavity cooling if a suitable design for the installation of the BIPV systems is considered.

In general, various correlations in the form of $Nu_x = C{Re_x}^a$ are adapted from heat convection of flat-plates to calculate the heat removal from the BIPV surfaces. However, these correlations demonstrate a high discrepancy with realistic conditions due to a more complex flow around BIPVs in comparison with the flat-plate scenarios. This study offers a significantly more reliable correlation using computational fluid dynamics (CFD) technique to visualize and thus investigate the flow characteristics around and beneath BIPVs. The CFD model is comprehensively validated against a particle velocimetry and a thermography study by (Mirzaei, et al., 2014) and (Mirzaei & Carmeliet, 2013b). The velocity field shows a very good agreement with the experimental results while the average surface temperature has a 6.0% discrepancy in comparison with the thermography study. Unlike the former correlations, the coefficients are not constant numbers in the newly proposed correlation, but depend on the airflow velocity.

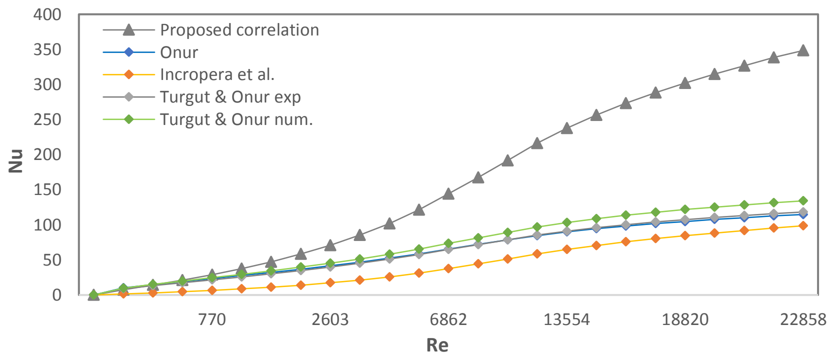

The performance of the newly developed correlation against precedent regressions (upstream velocity = 1m/s)

Keywords: Building; Photovoltaics; CFD; cavity cooling; wind-driven, surface temperature

1. INTRODUCTION

The utilization of photovoltaics (PV) has been continuously growing within the power sector and shows a phenomenal increase among all renewable energy sources over the last five years (Renewable Energy Policy Network for the 21st Century (REN21), 2014). Building-integrated photovoltaics (BIPV) systems, in particular, are one of the most promising applications of solar power technologies and offer considerable potential in responding to building energy demands. Roof-mounted applications of BIPV are currently holding the dominant position in all BIPV markets with a share of 80%. The rest of the market is mainly focused on facade integrated technologies (Krawietz, 2011). A typical roof-mounted BIPV system is assessed to be capable of supplying 14.5-57.8% of a building's energy demands, depending on the local available solar yields, mounting geometry and climatic weather conditions (International Energy Agency (IEA), 2002).

The electrical performance of a solar power panel can be predicted from a linear expression with known reference data measured at standard testing conditions (STC) - where solar radiation is $1000W/m^2$ at ambient temperature, $T_a = 25$°C. However, the efficiency of the silicon-based PV panels, as the dominant type of photovoltaic technology in the market, drops inversely with increasing cell temperature, also known as operating temperature. The decline ratio is addressed in many studies and is most likely to vary from 0.1 to 0. 5%/°C (Skoplaki & Palyvos, 2009). This indicates that cooling is becoming an essential technique to maintain the BIPV electrical performance, especially in hotter climates.

A variety of strategies has been proposed to enhance heat removal from solar cells, including the circulation of water flow through the BIPV's front surface, utilization of hybrid systems with thermal collectors, and using forced ventilation through the cavity (Krauter, 2004; Enteria & Akbarzadeh, 2013). Natural winds around the stand-off mounted BIPV can also assist the cooling by placing a sufficient air cavity to remedy the lack of convection at the rear side. Skoplaki and Palyvos (2009) summarize the current analytical correlations used for the determination of the operating temperature.

The main challenge in predicting the thermal behavior of the BIPV corresponds to the complex airflow regimes around these panels. Many studies in this area have been carried out both experimentally and numerically. For example, the Nominal Operating Cell Temperature (NOCT) defined in nominal terrestrial environment conditions and the Sandia National Laboratories (SNL) model are two common mathematical correlations that have been developed from empirical datasets (King, et al., 2004). The latter is preferable to the former as it encompasses both the wind effect and the solar radiation intensity (King, et al., 2004). Nonetheless, both of these models prove weak in understanding the effects of wind direction and terrain characteristics on the wind profile as well as the influence of the cavity size of the mounted BIPV. D'Orazio, et al. (2014) assessed these two models by comparing them with in situ experiments for three different roof installations: fully integrated and stand-off by 0.2m and 0.04m cavity sizes. The SNL model overestimates the back surface temperature in all scenarios. On the other hand, for all scenarios calculated by NOCT model overestimations of the heat removal from rear side were found to be significant on sunny, breezy days while on a typical windy day the predicted values were lower than measurements for stand-off BIPV. The largest deviations between the NOCT model and site measurement were 12°C and 8°C, respectively. The NOCT model was around 2.5% more accurate in its projection of the annual energy production in comparison with the SNL model. It was also recommended by D'Orazio, et al. (2014) that a 0.04m cavity gap is enough to supply sufficient cooling to the BIPVs in a typical Mediterranean climate.

Similar investigations on the effect of the cavity gap are carried out in several simulation studies. For example, Guiavarch and Peuportier (2006) used a commercial tool, COMFIE, to test the dynamic performance of three different BIPV installation methods on roofs: rack mounted, stand-off and shingling without an air cavity. Mono-crystalline and amorphous silicon solar cells were examined in two climates, Paris and Nice, with a vertical façade application for a social residential building and an inclined roof application for a single family house. Annual PV productivity was forecast to have a 6% increase with the excess heat from the back ventilation employed for space preheating purposes. Shingling was found as the least preferable option having both low yields and efficiency. In another study, Mei et al. (2003) utilized a building energy simulation tool (TRNSYS) to model the thermal condition of façade integrated photovoltaic panel with forced air cavity ventilation. The intention was to use the air heated up in the cavity for heating purposes during winter time.

Computational fluid dynamics (CFD) was broadly used to investigate the cavity cooling, taking into account the BIPVs performance by in detail representations of velocity, temperature and turbulence fields. An example is shown in the research by Li and Kavara (2012) where they recommended the use of the Renormalization Group (RNG) k-ε model as turbulence model to provide a better overall performance in comparison with other turbulence models for an unglazed transparent collector with PV/T systems under forced convection. Controversially, Getu et al. (2014) indicated that although k-ε models could provide a more accurate prediction for air and insulation layer temperature in comparison with the k-ω model, the latter has strength in prediction of the temperature distribution. The utilized k-ε model was based on the assumption of the presence of high turbulence, however leading to less agreement with the experimental scenario conduced in lower airflow velocities. The drawback of k-ω model was mentioned to be its instability, depending on the free stream ω value generated by the leading edge effect as discussed by Liao et al. (2007). Liao et al. (2007) conducted a CFD study to model the cavity cooling performance of a façade with integrated hybrid solar/thermal system. Experimental measurements were obtained using particle image velocimetry (PIV) for the validation of the CFD model. By using of computational results, a regression relation was proposed for the surface heat transfer (convection coefficient) in addition to a correlation with Nusselt number (Nu) against average air speed and cavity size. The predicted channel flow velocity, however, was higher than the measured values, also resulting into stronger predicted turbulence in comparison with the measurements.

In another study, Wilson and Paul (2011) ran a series of simulations for different air cavity sizes and tilt angles. The BIPV was tested by alteration of the tilt angle from 15° to vertical placement followed by nine cavity aspect ratios (cavity length to its height), ranging from 4.8–120, at upstream flow velocities of 0, 1, 2 and 3m/s. The optimum mounting option for the BIPV system was found to be a 90° inclined panel with a large air cavity under buoyancy dominant ventilation. The maximum electrical efficiency was observed to be about 10.7-10.9% though this number could be further improved by 0.5-1% with mixed mode convection. A noteworthy observation was that the BIPV operating temperature was more sensible to inclination in the context of natural convection, but changed little under mixed cavity ventilation. In a similar study, Gan (2009a) (2009b) developed a CFD model to explore the thermal performance of the BIPV in different mounting geometries, including roof pitch, cavity size and number of PVs. Unlike the study by Wilson and Paul (2011), the flow regime was assumed to be in the turbulent regime rather than laminar. The conducted parametric study revealed that cavity cooling cannot be improved after a certain threshold for the air cavity size. Moreover, stepped multi-panels were recommended as a preferable arrangement to achieve better cavity air circulations in comparison with a long single panel. A high risk of hot spot occurrence near the top edge of the panels was also observed with a maximum temperature being detected as over 85°C above the ambient temperature of London during the summer.

In another CFD study, Koyunbaba, Yilmaz and Ulgen (2013) validated a model to simulate the hourly performance of a façade integrated photovoltaic system in combination with a Trombe Wall using in situ measurements. The computational results were validated to predict temperature profiles of the system in correlation with its power output using the recorded datasets.

Jubayer, Karava and Savory (2010) developed a 3D CFD model of a BIPV/T system integrated into a 30° inclined roof of a low rise building. The investigation was mainly focused on the velocity field by comparison of the forced convective heat transfer using the Nusselt (Nu) number normalized by Reynolds (Re) number and studying various roof inclinations, wind angles, upstream roughness and turbulent intensities (Karava, et al., 2012). It was observed that turbulent kinetic energy (TKE) generally decreases with distance above the surface and also with the distance from the leading edge. Moreover, it was concluded that the buoyancy dominant flows, with Richardson (Ri) number within the range of 0.9-7, were likely to provide a 14% improvement in convective heat transfer.

As it was discussed in the mentioned studies, previous CFD researches of BIPV mostly focused on the cavity region with a fixed parallel flow, and only minimally include the impact of the entrance flow when wind is entering as a non-parallel flow. In other words, the microclimate around and within the BIPV's cavity can play a significant role in the heat removal mechanism from such panels. This effect is widely simplified in previous studies with 2D channel flow where the crucial impact of the approaching wind direction is neglected. Moreover, the velocity field was mainly predicted with correlations associated with parallel flow above a flat-plate. The overheating on surfaces of BIPV panels, however, could lead to fairly different phenomena, particularly in the case of buoyancy dominant flows. This study, therefore, aims to develop a more detailed model to calculate the heat removal from roof integrated PVs. The developed model is firstly validated using a comprehensive wind tunnel experiment by (Mirzaei & Carmeliet, 2013b) and (Mirzaei, et al., 2014). The reliability of the developed CFD model is further assessed by the demonstration of a systematic comparison of both the velocity and temperature fields. By utilization of a series of simulations, a new correlation model is proposed to predict BIPV's surface temperatures based on the airflow velocity.

2. METHODOLOGY

The developed CFD model was created similarly to an experimental study by (Mirzaei & Carmeliet, 2013b) and (Mirzaei, et al., 2014) as demonstrated in (Fig. 1). In this wind tunnel measurement, a PV panel was integrated into the windward roof of an isolated prototype building with a 1:20 scale to represent a fully-sized building with dimensions of H=11.6m × L=12.0m × W=11.3m. The PV panel was mounted parallel to the 45^{o} roof with a 30mm air cavity and facing normal to a solar simulator placed upstream at a distance of 800mm. The solar simulator was turned on to achieve radiation intensities of 150, 300 and 600W/m^2 on the PV surface placed against upstream velocities of 0.5, 1 and 2m/s. It is noteworthy to mention that the physical model was placed in a long atmospheric wind tunnel with cross section of 1.3m height and 1.9m width. The wind tunnel has an overall length of 25 m to ensure the supplied air to reach fully-developed boundary layer conditions. Furthermore, the PV's surface temperature was monitored by an infrared camera (IRC) placed upstream, far from building, with a thermal pile attached on the surface and several thermal couples on the front and rear of the PV panel. Particle image velocimetry (PIV) was employed to capture the velocity field around the PV panel (Mirzaei & Carmeliet, 2013b; Mirzaei, et al., 2014).

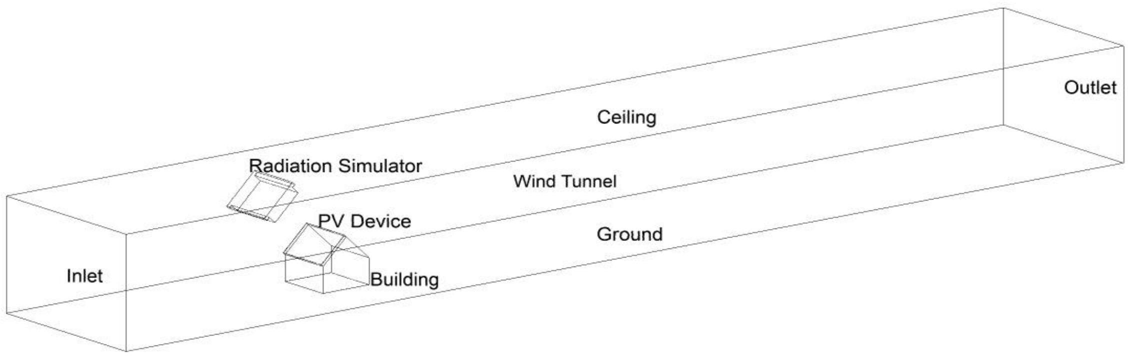

Fig. 1. CFD domain of the wind tunnel experiment by (Mirzaei & Carmeliet, 2013b) and (Mirzaei, et al., 2014)

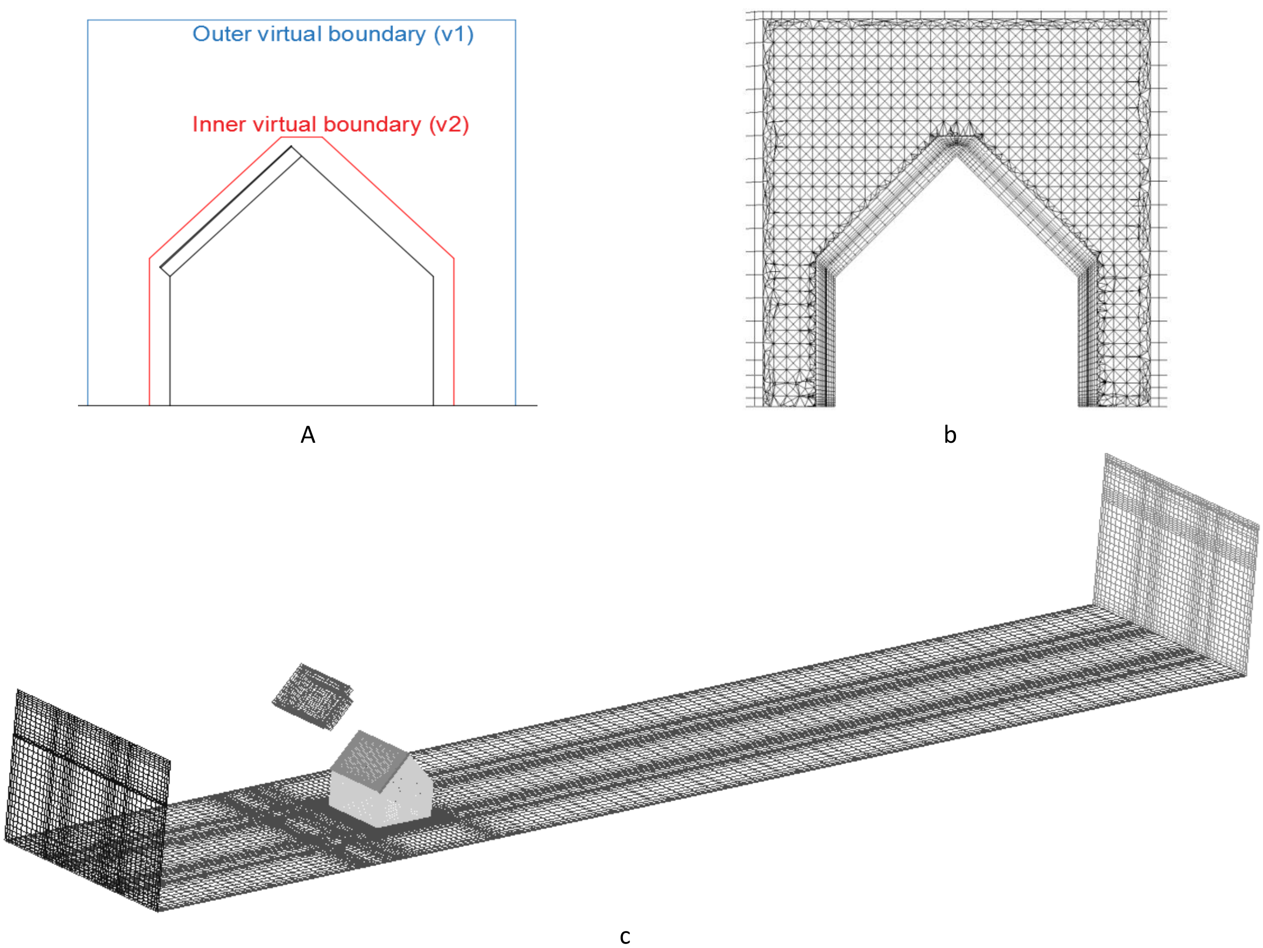

Fig. 2. (a) inner and outer virtual domains (b) Hybrid grids of the object region (c) surface mesh of the 3D BIPV model

As it can be seen in Fig. 1, the computational domain is stretched with 5H and 15H toward the upstream and downstream directions of the building, H being the height of the building prototype and equal to 0.58m. This is in alignment with the recommendations of the best practice rules in COST (Franke & Baklanov, 2007) and AIJ (Tominaga, et al., 2008). To minimize the computational cost, a hybrid mesh was generated around the building prototype (Mirzaei & Zhang, 2015). Fine near-wall cells were employed to obtain a high resolution result inside the boundary layer while the outer region was covered by a coarser structured grid. The buffer layer was filled by unstructured grids as can be seen in Fig. 2a. As depicted in Fig. 2b, two virtual boundaries were created at the inner and outer surfaces of the buffer layer to match the hexahedral and tetrahedral nodes; this procedure was a challenging part in the development of the hybrid mesh. The mesh was dense at the solid boundary with first layer size of 0.0025m and then became gradually coarser toward the outer layer with an inflation ratio of 1.2. The object region, including the near-wall and buffer layers, was assessed to achieve a high agreement with the experimental measurements.

A CFD simulation was conducted in this study using ANSYS FLUENT 15.0 while Reynolds Averaged Navier-Stokes (RANS) was adapted to solve the Navier-Stokes equations. Standard k-ε was used as the turbulence model as it is widely suggested in similar investigations due to a tremendous lower computational cost when compared with more accurate models such as Large Eddy Simulation (LES) (Mirzaei & Rad, 2013). The RANS governing equations can be written as below (Mirzaei & Haghihat, 2011):

$$for\ Continuity: \quad \frac{\partial}{\partial x_j}(U_j) = 0 \qquad (1)$$

$$for\ Momentum: \quad \rho U_j \frac{\partial}{\partial x_j}(U_i) = -\frac{\partial_p}{\partial x_i} + \frac{\partial}{\partial x_j}\left[(\mu + \mu_t)\frac{\partial U_i}{\partial x_j}\right] \qquad (2)$$

where U is the flow velocity, ρ is the fluid density, *i, j*= 1, 2, 3 and μ_t is the turbulent viscosity and represented as below:

$$\mu_t = C_\mu \rho \frac{k^2}{\varepsilon} \qquad (3)$$

where C_μ is a constant, k is the turbulence kinetic energy and ε is the dissipation rate of k.

A wide range of variation in RANS models, including Standard (Sk-ε), Realized (Rk-ε) and Renormalization-group k-ε (RNGk-ε), were tested in this study and it was found that the Sk-ε model shows a better agreement with experimental results. Also, the solutions are found to have a better stability in reaching a faster convergence compared to the other models. The enhanced wall function was utilized in this study. The Sk-ε model solves the turbulent flow using the transport equations presented as follows (Launder & Spalding, 1972):

$$\frac{\partial}{\partial t}(\rho k)+\frac{\partial}{\partial x_i}(\rho k U_i)=\frac{\partial}{\partial x_j}\left[\left(\mu+\frac{\mu_t}{\sigma_k}\right)\frac{\partial k}{\partial x_j}\right]+G_k+G_b-\rho\varepsilon-Y_M+S_k \qquad (4)$$

$$\frac{\partial}{\partial t}(\rho \varepsilon)+\frac{\partial}{\partial x_i}(\rho \varepsilon U_i)=\frac{\partial}{\partial x_j}\left[\left(\mu+\frac{\mu_t}{\sigma_\varepsilon}\right)\frac{\partial \varepsilon}{\partial x_j}\right]+C_{1\varepsilon}\frac{\varepsilon}{k}(G_k+C_{3\varepsilon}G_b)-C_{2\varepsilon}\rho\frac{\varepsilon^2}{k}+S_\varepsilon \qquad (5)$$

Where G_k and G_b are the generated k terms with respect to the mean velocity gradient and buoyancy, respectively; σ represents the turbulent Prandtl number; Y_M represents the dilatation dissipation, S_k and S_ε are additional source or sink terms for k and ε; $C_{1\varepsilon}$, $C_{2\varepsilon}$ and $C_{3\varepsilon}$ are constant values.

The short wave radiation was simulated using solar ray tracing model with only the PV panel participated in the calculations. The emissivity of PV panel was set to be 0.9 as used in the wind tunnel experiment. The energy equation was utilized to obtain the temperature field as below:

$$\frac{\partial}{\partial t}(\rho E)+\frac{\partial}{\partial x_j}\left(U_j\rho E\right)=-p\frac{\partial}{\partial x_j}\left(U_j\right)+\frac{\partial}{\partial x_j}\left(k_{eff}\frac{\partial}{\partial x_j}(T)\right)+\Phi+S_h \qquad (6)$$

where k_{eff} is the effective turbulent thermal conductivity, Φ represents the dissipation function, and S_h is volumetric sources. In this equation, the total energy is defined as follows:

$$\mathrm{E}=\mathrm{h}-\frac{p}{\rho}+\frac{U^2}{2} \qquad (7)$$

where h and p are sensible enthalpy and pressure of the ideal gas, respectively.

Treatments of the boundaries are further described in Table 1. The airflow was modeled to be introduced into the wind tunnel normal to the inlet boundary and with a uniform profile. The turbulence intensity at both inflow and outflow was calculated by the following equations (ANSYS FLUENT, 2009):

$$\mathrm{I}=0.16\mathrm{Re}_{dh}{}^{-1/8} \qquad (8)$$

$$\mathrm{Re}_{dh}=\frac{\rho U d_h}{\mu} \qquad (9)$$

where d_h is the hydraulic diameter. The experiments were performed at room temperature T_a = 25°C with the air density ρ =1.2245 kg/m^3; the turbulence intensities were thereby assigned as 4.1%, 3.8% and 3.5% for the case with upstream velocities of 0.5, 1 and 2m/s, respectively. A sensitively analysis of the impact of the turbulence intensities on the velocity, temperature and turbulence fields was performed and justified the above mentioned choices.

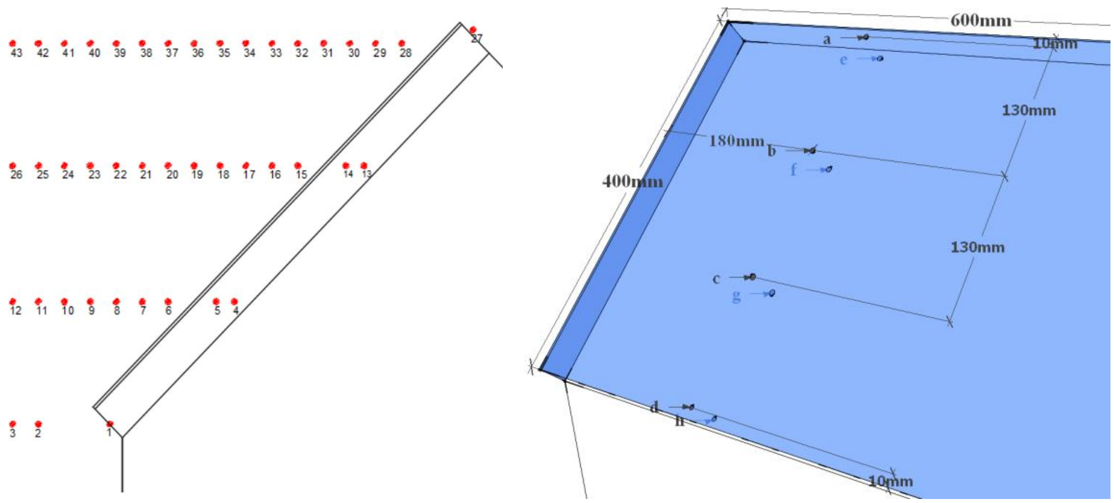

a b

Fig. 3. Distribution of (a) 43 points for the velocity field, and (b) 8 points for the temperature field validation

Table 1. Computational setting for the CFD model

Boundary	Type	Treatment
Ground/Ceiling/laterals walls/Building surfaces/Radiator/PV holder/PV back and lateral surfaces	Wall	No-slip Not included in the radiation model
Front surface of PV	Wall	No-slip Emissivity = 0.9
Inflow	Velocity inlet	Constant Normal to the boundary Turbulent Intensity Hydraulic diameter =1.54m
Outflow	Pressure outlet	Gauge pressure =0 Turbulent Intensity Hydraulic diameter =1.54m
Near-wall treatment	Enhanced Wall function	
Pressure-Velocity Coupling	SIMPLE	
Discretization scheme		
Pressure	Second Order	
Momentum	Second Order Upwind	
Turbulent Kinetic Energy	First Order Upwind	
Turbulent Dissipation Rate	First Order Upwind	
Energy	Second Order Upwind	

Before proceeding to the validation stage, a mesh sensitivity test was conducted using three sets of mesh with 1.1m, 1.3m and 2.1m cells while cell densities were also altered in each mesh to reach a suitable model. The selected mesh was generated with about 1.3million cells. To maintain an acceptable smoothness ratio, extensive effort has been conducted to achieve a stretching ratio between two consecutive meshes of 1.2-1.5 as suggested by COST and AIJ ((Franke & Baklanov, 2007; Tominaga, et al., 2008). The convergence of 10^{-7} was also achieved for the energy equation whilst this number was 10^{-5} for the momentum and turbulent equations. Segregated solver algorithm SIMPLE scheme is used for pressure-velocity coupling in this study with combination of first and second order discretization schemes for different equations (Table 1). The wall-enhanced treatment was utilized on walls with average y+ for the solid boundaries inside the object region obtained to be below 7.5.

The validation was performed for both velocity and temperature fields associated with the experimental study. The velocity field was validated against a series of isothermal and non-isothermal cases with a radiation intensity of 600W/m^2 emitted onto the PV surface. The air flow pattern at a section parallel to the upstream flow was monitored by PIV technique as described by (Mirzaei, et al., 2014). The comparison of the velocity magnitude and the entire flow pattern was performed at 43 selected points on the longitudinal section of the BIPV as illustrated in Fig. 3a. In terms of the thermal field validation, in addition to the mean and pattern of the surface temperature, two arrays of points were assigned to the front surface of the PV (a-d) as well as the building's roof (e-h) as shown in more detail in Fig. 3b.

The effect of upstream velocity magnitude and solar radiation on the convective heat removal from both surfaces of the BIPV panel was studied using the Nusselt number as defined below:

$$Nu_x = \frac{hx}{K} = f(Re, Pr) \qquad (10)$$

where *h* is the convective heat transfer coefficient, *x* is the distance from the edge of the PV, K is the thermal conductivity of air, and *Pr* is the Prandtl number. As the value of *Pr* for airflow remains fairly stable, it was assumed to be equal to 0.71 in the experimental conditions.

3. RESULTS AND DISCUSSION

3.1 Validation of the velocity field

The comparison of velocity normalized by the inlet velocity at the selected points of Fig. 3 between simulation and experiment is shown in Fig. 4. In general, under isothermal conditions, the CFD model is more likely to underestimate the velocity with the highest deviation of approximately 23.1%, 20.1% and 16.7% in upstream velocities of 0.5, 1 and 2m/s, respectively. The average discrepancy is calculated to be approximately 5.7% in the cavity, 10.3% in the upstream region and 9.5% in the whole domain. When the solar simulator emits radiation with an intensity of 600 W/m^2 on the PV panel and the upstream velocity is 0.5m/s, the average and maximum differences inside the cavity are obtained about 14.7% and 32.1%, respectively. It can be concluded that the average accuracy of the CFD model increases in the higher upstream velocities as 10.1% and 9.9% of average discrepancies have been calculated for the velocities of 1m/s and 2m/s, respectively. The maximum error is almost halved (16.9%) when the upstream flow is 2m/s.

The average error of the velocity field for non-isothermal scenarios is about 13.2% in the cavity, 7.2% in the upstream region and 8.0% in the whole domain. One of the main reasons for this discrepancy can be attributed to the limitation of the Sk-ε turbulent model, which is based on the assumption of a high turbulence flow regime (Getu, et al., 2014; Mirzaei & Carmeliet, 2013a). Evidently, the upstream velocities in the larger Re regimes, thereby, provides better predictions.

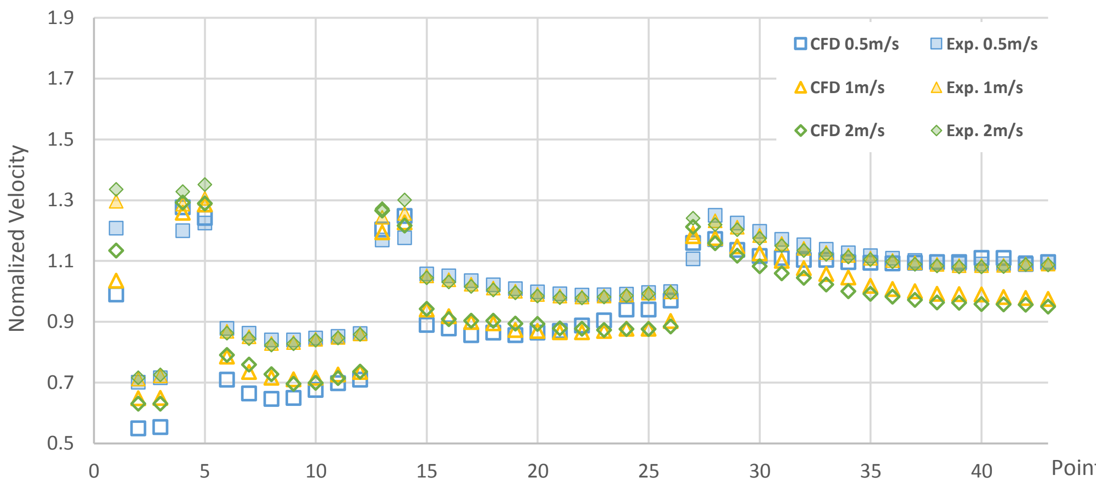

(a)

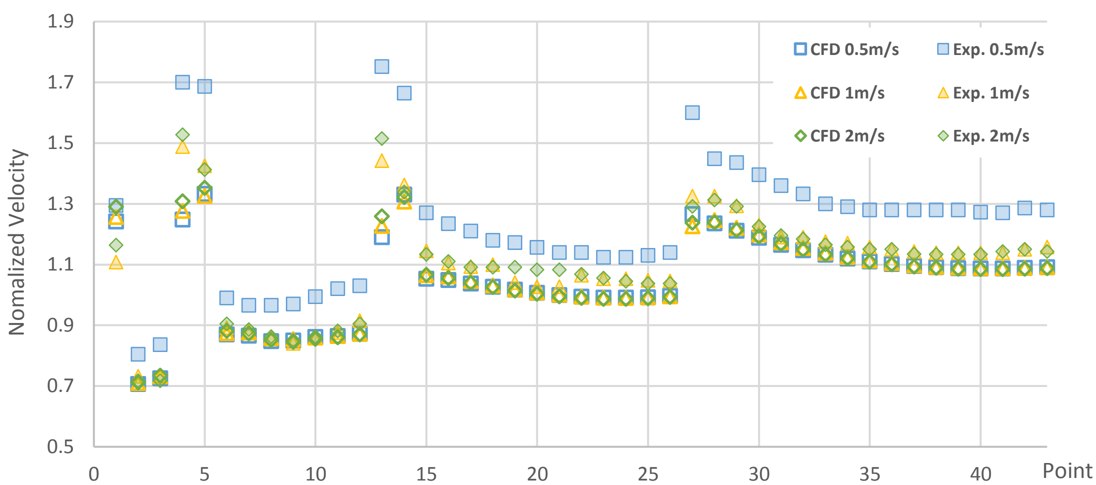

(b)

Fig. 4. Comparison of the normalized velocity at 43 points between CFD and experimental results in different upstream velocities (0.5 m/s, 1 m/s and 2 m/s) for (a) isothermal and (b) non-isothermal scenarios

In contrast with the non-isothermal scenarios, when the solar simulator is turned off, high errors can be observed at the region located in front of the panel. The PIV uncertainty in extracting the experimental values can be up to 3% and, hence, can be considered one of the potential sources of the discrepancy in the validation process.

The velocity contours obtained from the PIV experiment (Mirzaei, et al., 2014) and CFD modeling are compared in Fig. 5 for isothermal and Fig. 6 for non-isothermal scenarios. All velocity patterns reveal to be fairly similar to each other while it can be observed from the isothermal scenarios that a slightly larger vorticity is present at the windward wall of the building in the experiment in comparison with the CFD modeling as shown in Fig. 5. This can be partially explained as the lack of laser beam illuminate this at this region as required for a high resolution visualization. Furthermore, Fig. 6 reveals that the CFD results show less acceleration of the airflow at the entrance of the cavity compared to the measured results. The error is mitigated when a stronger inflow is employed, which can again be associated to the defect of the Sk-ε turbulent model in predicting low turbulence scenarios. This point is further discussed in the turbulence validation section where an error of 14.7% is obtained for turbulent kinetic energy in the low upstream velocity of 0.5m/s. This number, however, reduces in the higher upstream velocities of 1m/s and 2m/s to 4.6% and 4.8%, respectively.

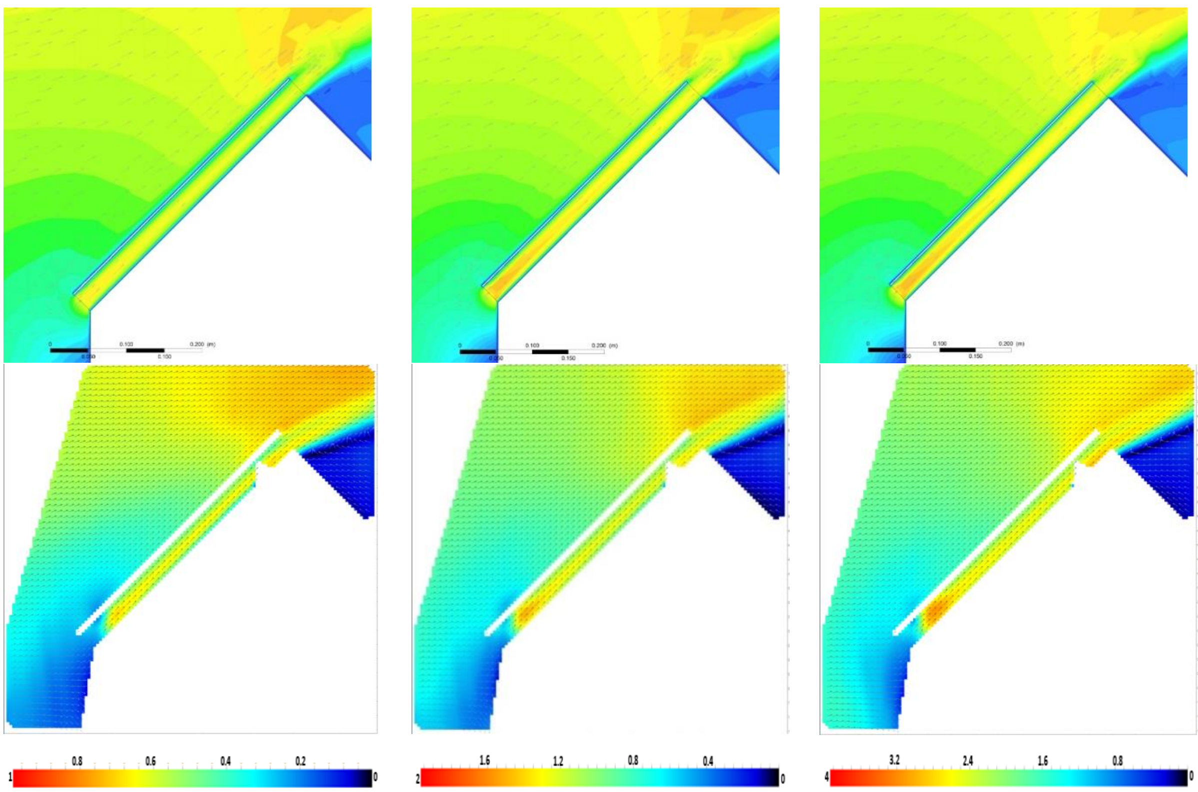

(a) (b) (c)

Fig. 5. Comparison of the velocity contour between (top) computational and (bottom) experimental (Mirzaei, et al., 2014) studies for isothermal scenarios with upstream velocities of (a) 0.5m/s, (b) 1m/s and (c) 2m/s

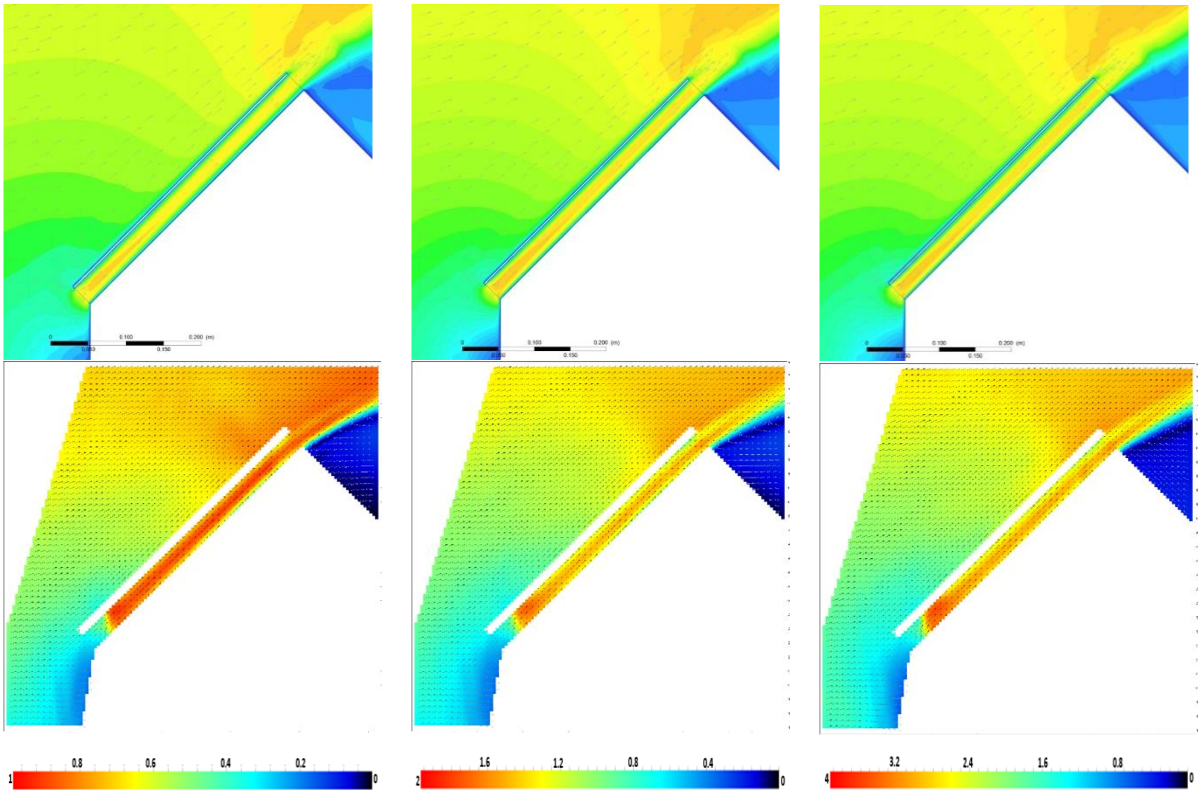

(a) (b) (c)

Fig. 6. Comparison of the velocity contour between (top) computational and (bottom) experimental (Mirzaei, et al., 2014) studies for non-isothermal scenarios with upstream velocities of (a) 0.5m/s, (b) 1m/s and (c) 2m/s

3.2 Validation of the temperature field

The reliability of the CFD model in predicting the thermal field is investigated in this section using the mean surface temperature and the temperature patterns of the various scenarios in the presence of the radiation intensity generated by the solar simulator. As it can be seen in Fig. 7**Fig. *7***, the simulated temperature distributions on the front surface of the BIPV match fairly well with those captured by infrared camera (Mirzaei & Carmeliet, 2013b). Higher temperatures usually occur near the top edge of the PV panel as the air is warmed by the hot panel when it removes heat from the panel along its path until reaching the higher edge of the cavity. It should be remarked that the experiment was designed with six radiative lamps in array of 2×3, explaining why the radiation intensity was not completely homogeneous on the surface of the panel. On the other hand, the PV panel was assumed to be heated by a homogeneous radiation intensity in the CFD simulation, which can explain a potential source of the discrepancy that can be seen between the experimental and computational results in Fig. 7.

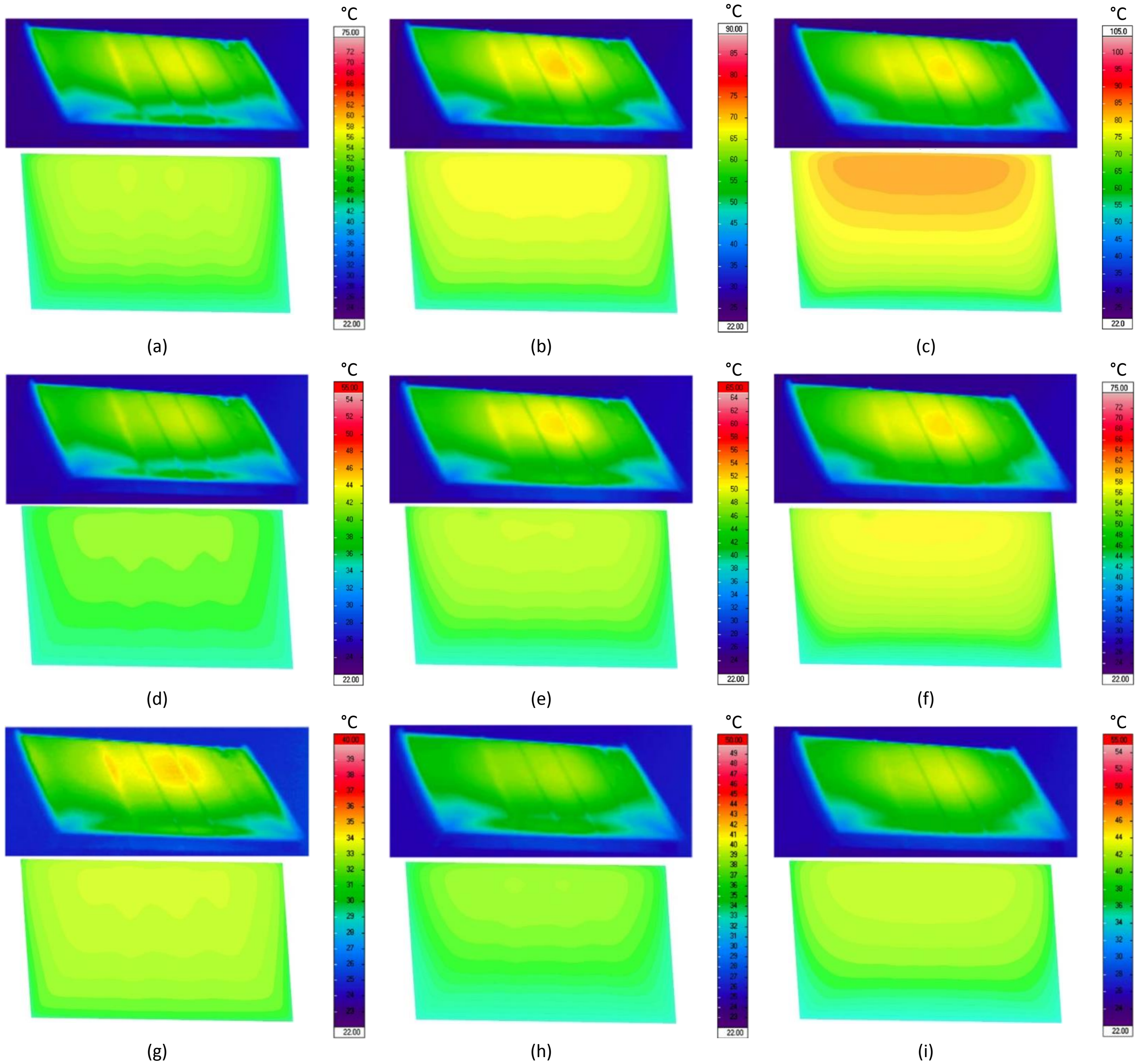

Fig. 7. Comparison of the temperature contour of the front surface of the BIPV between (top) experimental (Mirzaei & Carmeliet, 2013b) and (bottom) computational studies for scenarios with different upstream velocities of (a, d, g) 2m/s, (b, e, h) 1m/s and (c, f, i) 0.5m/s when the radiation intensity is (a-c) 600W/m^2, (d-f) 300W/m^2 and (g-i) 150W/m^2

In general, it can be concluded that the CFD model is successful in simulating the mean temperature of the PV panel's front surface with an average error of about 6.0% in comparison with the measurement result. The CFD model shows also a good performance in the prediction of the local temperatures at the front surface (points a-d) where the average accuracy is calculated to be over 95.0%. The highest accuracy is 98.1% and is associated with the scenario with upstream velocity of 1 m/s and 600 W/m^2 radiation intensity. A part of the large error observed in the prediction of temperature for the points e-h on the building roof surface can be attributed to the fact that these points are not exactly located at the roof surface in the simulation, but 1mm above it. Moreover, the thermal conductivity of the material assigned in the simulation can be slightly different from the real value of the experiment, which again can be a source of the observed deviation between experiment and simulation. Although an aluminum coating was applied on the windward wall of the building prototype to prevent the absorption of an excess irradiance (Mirzaei & Carmeliet, 2013b), the building surface could still absorb heat to some extent, which can be assumed as another cause of the slight mismatch between experimental and computational results. In other words, the air could already be preheated after encountering the building wall prior to entering the cavity. This phenomenon was neglected in the CFD modeling as the building was set to be isolated from solar radiation.

In addition, the buoyancy-dominated flow in the cavity imposes technical difficulties for the turbulence modeling. For instance, if the upstream velocity is fixed to be 2m/s, lower accuracy is attained for the high radiation intensity of 600W/m^2, with an average error for points e-h of 9.7%, compared to the scenario with radiation intensity of 150W/m^2 where the average error is only 1.6%. The error shown in the prediction of the roof temperature can therefore be attributed to the underestimation of the air velocity in the cavity, which leads to smaller predicted levels of turbulence which is a weakness of the employed Sk-ε model as mentioned in an earlier section. Evidently, the scenarios with the higher upstream velocities demonstrate a better agreement in prediction of the roof temperature. The average errors are calculated to be about 1.6% and 7.8% with upstream velocities of 0.5m/s and 1m/s under the radiation intensity of 150W/m^2.

3.3 Validation of the turbulence field

Fig. 8 shows the turbulent kinetic energy (TKE) patterns for the scenarios under high intensity radiation of 600W/m^2 with different upstream velocities. Apparently, the TKE at the outlet of the cavity (near the edge of the region where leeward vorticity occurs) is found to be higher than at other locations in both the simulation and experimental results. The CFD model, however, underestimates the TKE in the circulation region attached to the back surface of the PV panel at the entrance of cavity, especially when air is induced at a low upstream velocity. This could be attributed to the employed k-ε turbulence model, which has difficulty in representing the TKE at the regions near the boundaries (Puleo, et al., 2004; Tominaga, et al., 2008). Also, there is an obvious overestimation of TKE by the simulation in the upstream region of the roof, as can be seen in Fig. 8, indicated by lighter colors above the roof. Although the employment of more accurate models such as LES is preferable to enhance the TKE prediction, the computational cost will drastically increase, which again justifies the utilization of the k-ε turbulence model in this study (Franke & Baklanov, 2007).

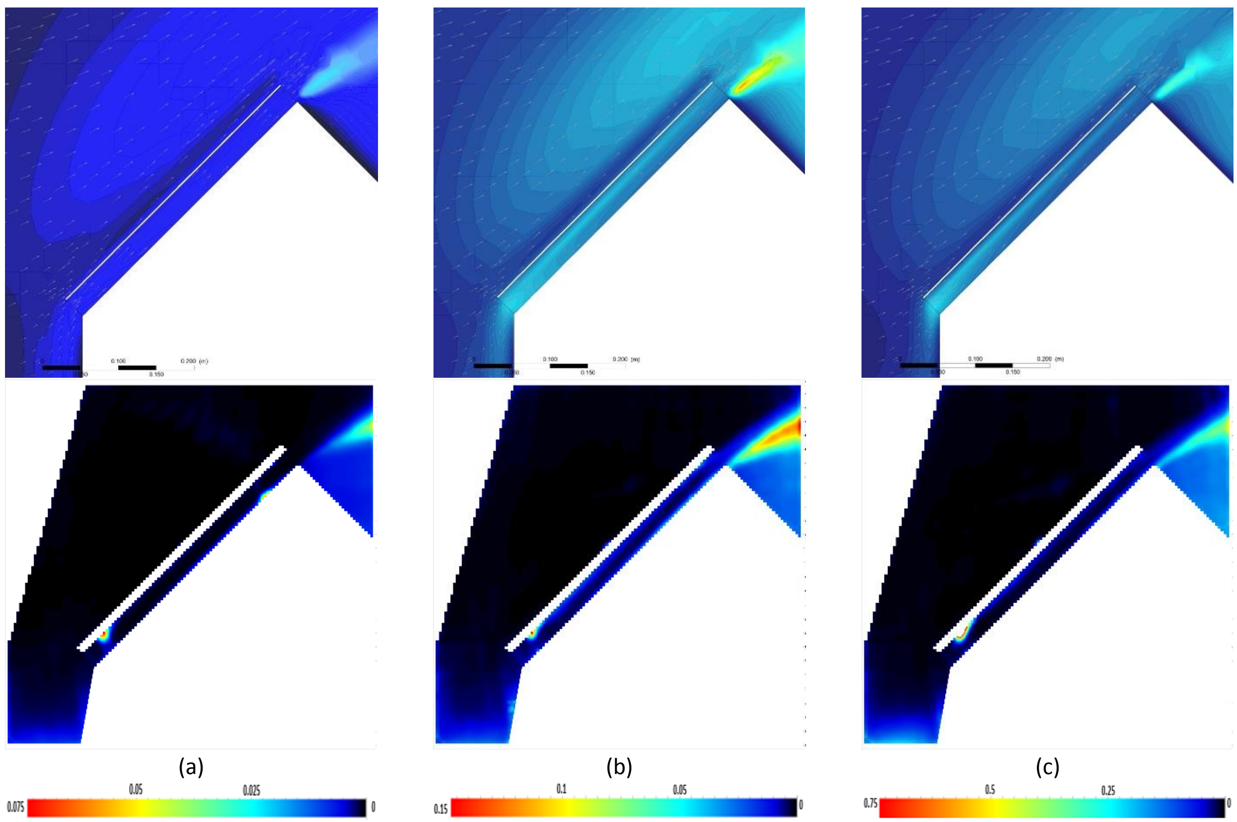

Fig. 8. Comparison of TKE contour between (top) computational and (bottom) experimental (Mirzaei, et al., 2014) studies for non-isothermal scenarios with upstream velocities of (a) 0.5m/s, (b) 1m/s and (c) 2m/s

3.4 Convective heat transfer

Convective heat transfer from the flat-plates is traditionally expressed with the following equation (Onur, 1993):

$$Nu = cRe^{a} \qquad (11)$$

where *a* and c are the constant coefficients. These correlations are widely used to estimate the convective heat coefficient or Nusselt number associated with the PV panels. A summary of these correlations, which are in the form of the Equation (11), are presented in **Error! Reference source not found.**.

Table 2. Precedent correlations for Nusselt number or convective heat transfer coefficient

Authors	Correlations	Comments
McAdams (1954)	$\mathrm{h} = 5.7 + 3.8\mathrm{U}$	For forced convection over an inclined flat plate
Onur (1993)	$\ln(Nu) = 0.065 + 0.466\ln(Re)$	For turbulent flow over a 45° inclined plate with 0° yaw
Incropera, et al. (2006)	$Nu = 0.036Re^{0.8}\, Pr^{1/3}$	For turbulent flow
Turgut & Onur (2009)	$Nu_{experimental} = 0.782Re^{0.5}$ $Nu_{numerical} = 0.887Re^{0.5}$	For forced convection over a 45° inclined plate with 0° yaw

In this section, the convective heat transfer on two surfaces above and beneath the panel at a distance of 10mm is investigated by comparing the validated CFD results and the precedent correlations as listed in Table 2. Thus, the first layer of the mesh (0.0025m), in lines parallel to the stream-wise flow in both front and back surfaces, was used to investigate the Nusselt number at the BIPV surfaces. The Nusselt number based on CFD modeling was thereby calculated using Equation (10) applied at 25 local points along each line, ranging from 0 to 0.4m (from the bottom to the top edge of the BIPV excluding two-end points at the edge). It was found that the Nusselt number barely changes with radiation intensity as the effect of a higher heat transfer is compensated by a larger temperature difference between the surface and air. Similar patterns for different radiation intensities were correspondingly observed with a deviation less than 1%.

Fig. 9 compares the Nu numbers on the front surface of the PV between CFD results and precedent correlations for scenarios with the strongest radiation intensity, but different upstream velocities. Similarly, this comparison for the back surface is shown in Fig. 10. The Nu number at the back surface shows a better agreement to the precedent correlations compared to the front surface. Both surfaces, however, provide larger deviations from the existing correlations closer to the top edge where the Reynolds number (Re) increases.

Table 3. The comparison of the Nu obtained from CFD with the precedent correlations

Correlation	McAdams (1954)	Onur (1993)	Incropera, et al. (2006)	Turgut & Onur (2009)	
				Exp.	Num.
Deviation at front surface	59.0%	53.7%	80.8%	53.9%	50.1%
Deviation at back surface	56.3%	55.5%	76.2%	54.1%	51.9%

To check the validity of the precedent model against the proposed correlation, mean squared error for all correlations related to the CFD model has been calculated. It was observed that none of the correlations provide a close prediction as demonstrated in Table 3. The results show that the Nu number obtained with CFD simulation matches best to the existing correlation given by Turgut & Onur (2009) although it still shows a high standard deviation of 50% and 52% at front and back surface in comparison with the CFD prediction. The underestimation of Nu by the existing correlations can be attributed to their choice of the flow regime, e.g. Onur (1993) and Turgut & Onur (2009) used laminar flow rather than the turbulent regime. It also can be related to the type of the cavity ventilation. For example, the equation given by McAdams (1954) was determined for a vertically mounted panel seated in parallel wind, which implies a weak cavity ventilation at backside. In general, the Nusselt number is found to be more sensitive to the magnitude of the upstream velocity at the front surface, where the average ratio in change of the local Nu (ΔNu) to the change of the upstream velocity (ΔU) is approximately 37.8% in comparison with a ratio of 25.8%

for the back surface. The reason for this can be explained by a more buoyancy-dominated flow in the cavity compared to the front surface.

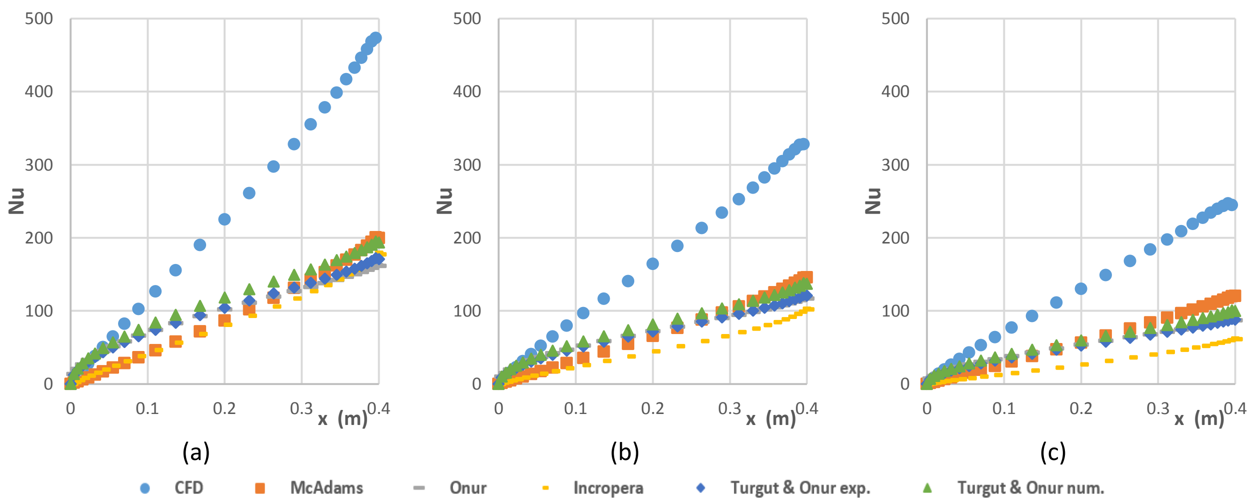

Fig. 9. Comparison of Nu at the front surface of the BIPV by CFD modeling and precedent correlations for different scenarios with radiation intensity of 600W/m^2 when upstream air is induced at (a) 2m/s, (b) 1m/s and (c) 0.5m/s

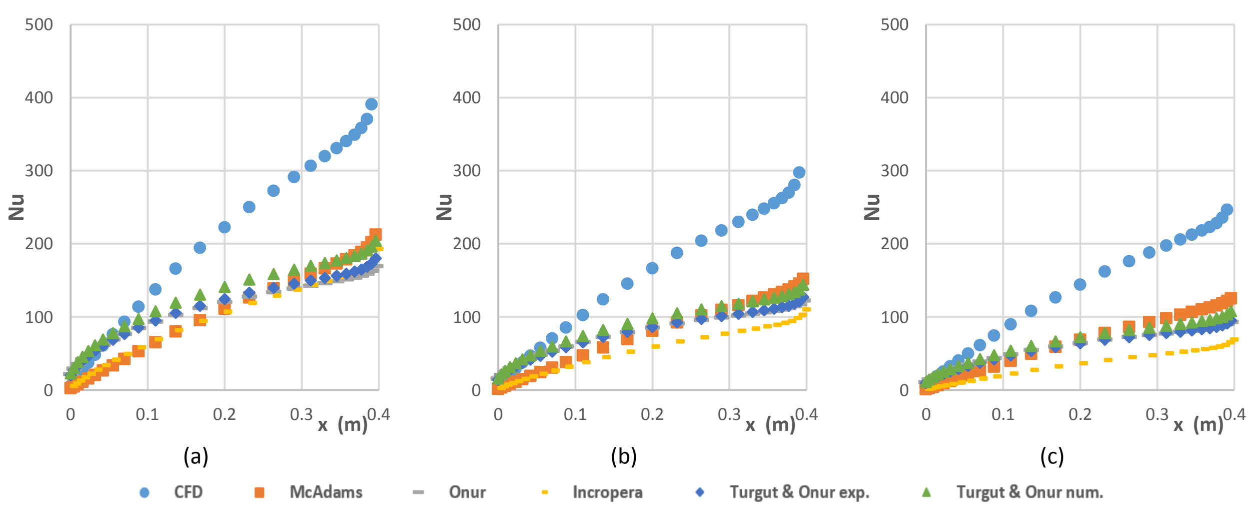

Fig. 10. Comparison of Nu at the back surface of the BIPV by CFD modeling and precedent correlations for different scenarios with radiation intensity of 600W/m^2 when upstream air is induced at (a) 2m/s, (b) 1m/s and (c) 0.5m/s

The simulated local Nu at the PV surfaces, as shown in Fig. 9 and 10, are utilized to develop a new correlation as a function of the Re number similar to Equation (9). The results are presented as a series of correlations in Table 4. The quality of the fitted correlations is evaluated using adjusted R-square, which is obtained to be above 0.99 and highly acceptable. The calculated Nu versus Re for different scenarios are also illustrated in Fig. 11.

These new correlations are also compared to the correlations of Table 2. Apparent underestimations of the Nu number by these correlations can be seen, especially for the higher Re numbers, occurring apart from the leading edge of the PV panel. Scenarios with lower upstream velocities are more likely to be dominated by convection heat transfer due to the stronger buoyancy effect at the surface. For the same velocity, the curves show larger deviations at the upper edge of the PV panel where there is a larger temperature difference between the panel and ambient due to the different radiation intensities. Also, from Fig. 11, it can be seen that the upstream velocity plays a more influential role than solar radiation intensity on the local Nu number. At an upstream velocity of 2m/s the curves for different radiation intensity almost coincide.

Table 4. Correlations of the simulated Nu versus Re for different scenarios

Upstream velocity (m/s)	Solar intensity (W/m²)	Correlations
0.5	150	$Nu_x = 0.4753Re_x{}^{0.6772}$
	300	$Nu_x = 0.2191Re_x{}^{0.7353}$
	600	$Nu_x = 0.09369Re_x{}^{0.7959}$
1	150	$Nu_x = 0.4567Re_x{}^{0.679}$
	300	$Nu_x = 0.2208Re_x{}^{0.7338}$
	600	$Nu_x = 0.09574Re_x{}^{0.7945}$
2	150	$Nu_x = 0.4368Re_x{}^{0.6802}$
	300	$Nu_x = 0.2247Re_x{}^{0.7307}$
	600	$Nu_x = 0.0971Re_x{}^{0.7927}$

At this stage a regression equation is proposed for the coefficients a and c in Equation 11 based on the correlations presented in Table 4. As discussed, the upstream velocity and temperature differences between the PV surface and ambient air are considered as the influential parameters, but the impact of the latter is found to be negligible as similar patterns for different radiation intensities are observed with a deviation of less than 1%. Therefore, the upstream velocity U can be considered as the only variable in the regression model for the purpose of simplification. The coefficients of the regression equation, with R-square of above 0.99, are obtained as below:

$$\begin{cases} c = 0.229U^2 - 0.8129U + 0.8055 \\ a = -0.03189U^2 + 0.1568U + 0.6084 \end{cases} \qquad (12)$$

where U is the flow velocity at the inlet.

The developed CFD model shows good agreement with the experimental results, however, it still contains a small level of discrepancy in the velocity (u±Δu) and temperature (T±ΔT) fields, which can potentially effect the calculation of the local Nu numbers and propagate more discrepancy into the predictions. Therefore, the certainty of the regression model in prediction of the local Nusselt number is investigated at this stage by considering errors Δu and ΔT in the calculations.

Fig. 12 presents a range of Nu and Re numbers calculated at each point according to the obtained Δu and ΔT of the previous section. This implies that the calculated local Nusselt number from the regression model should be within the bounded area as shown with two boundary lines in the same color for each scenario. The most probable uncertainty in the results is about 29.3% against upstream velocity of 0.5m/s and solar radiation intensity of 300W/m^2. In general, the proposed correlation is more likely to provide the local Nu with an acceptable uncertainty of below 20%. Apparently, the precedent correlations still fail to give an accurate estimation for the local Nusselt number as they all exist out of the bounded area. The main reason of the discrepancy associated to these models could be the treated flow regime to be laminar rather than turbulent.

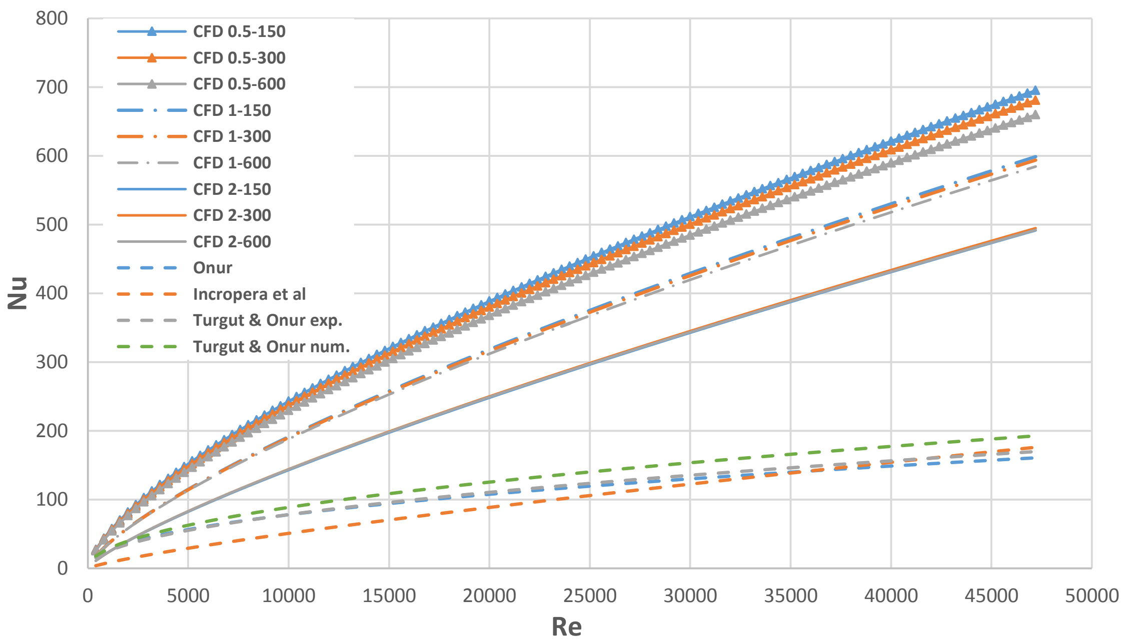

Fig. 11. Comparison of the CFD correlations of the local Nu versus local Re with those by the precedent studies for scenarios with inflow of 0.5m/s, 1m/s and 2m/s at radiation intensities of 150W/m^2, 300W/m^2 and 600W/m^2

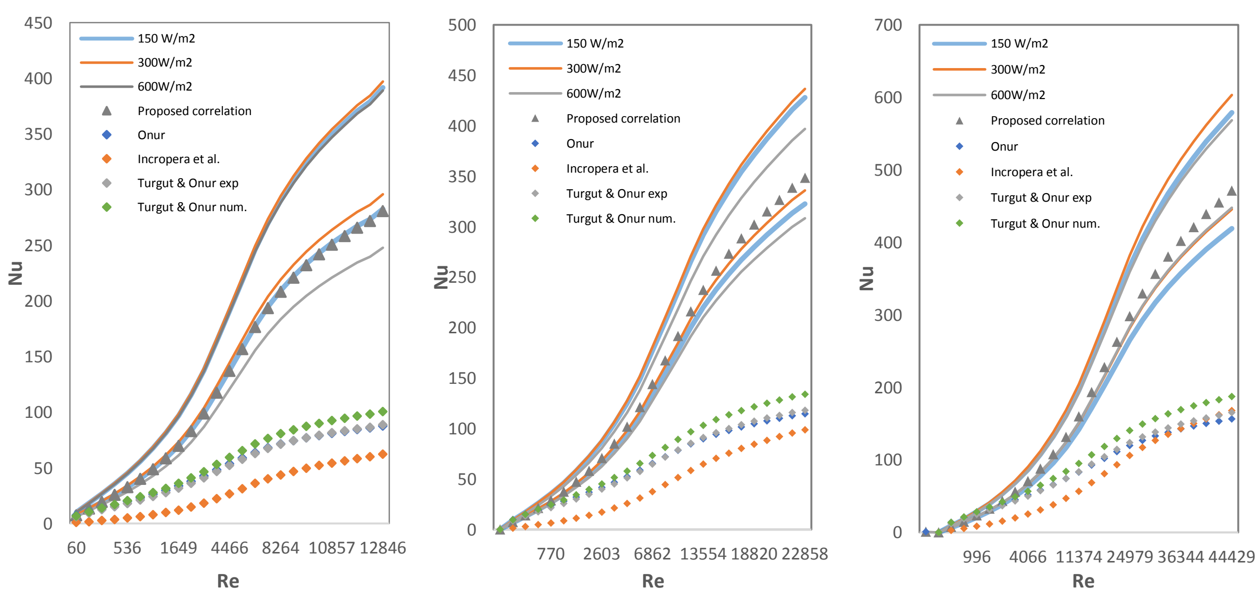

(a) (b) (c)

Fig. 12. The certainty of the estimated results by the obtained regression in comparison with the precedent correlations for scenarios with inflow velocity of (a) 0.5m/s; (b) 1m/s and (c) 2m/s.

4. CONCLUSION

In this study more accurate correlations to predict the surface temperature of the PV panels using the CFD technique are proposed. The new correlations were based on 3D CFD results, where the CFD model was validated against a comprehensive wind tunnel investigation of velocity and temperature patterns around a BIPV prototype. The main results of the validation procedure, found by comparing the computational and experimental data are summarized as follows:

- With increasing upstream velocity, a higher accuracy of the CFD modeling is observed. This is because the employed Sk-ε turbulence model is based on the assumption of a high Reynolds number. The average error for the prediction of the velocity field for the isothermal cases is about 9.7% and 8.0% for the non-isothermal scenarios.
- The simulated temperature distribution on the front surface of the panel shows good agreement with the experimental measurements while the average accuracy of the surface mean temperature is over 95.0%.
- The weakness of Sk-ε model is apparent in the representation of buoyancy-dominated flow and temperature distribution within the cavity for non-isothermal cases. The average error of the building roof temperature prediction is 6.1% for the highest radiation intensity of $600W/m^2$, and 3.8% for a radiation intensity of $150W/m^2$.
- In general, the model has shown weaknesses in capturing a high level of the TKE at the entrance of the cavity. An overestimation of TKE was observed at the front of the panel while the TKE is underestimated at the entrance of the cavity.

The Nusselt number is assessed in this study at the midlines of the front and back surface of the PV panel by comparing the Nu number values obtained by CFD to precedent correlations. Large deviations between the correlations and the CFD results are observed near the top edge of the PV panel where the Reynolds number is higher. It is found that the Nu value does not significantly depend on the radiation intensity. The Nu number at the back surface is found to be more sensitive to the upstream velocity than at the front surface. It is also found that the precedent correlations of the local Nusselt number fail to accurately describe the condition at front surface of the panel with an average error of over 50%. A new correlation is proposed in which the coefficients are function of the upstream velocity. The results of this study should be expanded in the future work to different cavity height and roof angles, and thus a more general correlation should be adapted when such factors are further included in surface temperature of the photovoltaic panels.

ACKNOWLEDGEMENT

The authors would like to express their gratitude to the faculty of the engineering of the University of Nottingham for the financial support.

REFERENCES

ANSYS FLUENT, 2009. *ANSYS FLUENT 12.0 User's Guide,* s.l.: ANSYS Inc..

D'Orazio, M., Di Perna, C. & Di GIiuseppe, E., 2014. Experimental Operating Cell Temperature Assessmnet of BIPV with Different Installation Configuration on Roofs under Mediterranean Climate. *Renewable Energy*, 6 3, pp. 378-396.

Enteria, N. & Akbarzadeh, A., 2013. *Solar Energy Sciences and Engineering Applications.* Boca Raton: CRC Press.

Franke, J. & Baklanov, A., 2007. *Best Practice Guidline for the CFD Simulation of Flows in the Urban Environment: COST Action 732 Quality Assurance and Improvement of Microscale Meterorological Models.* Hamburg: Meterological Inst..

Gan, G., 2009a. Effect of Air Gap on the Performance of Building-Integrated Photovoltaics. *Energy,* 34(7), pp. 913-921.

Gan, G., 2009b. Numerical Determination of Adequate Air Gaps for Building-Integrated Photovoltaics. *Solar Energy,* 83(8), pp. 1253-1273.

Getu, H., Yang, T., Athienitis, A. K. & Fung, A., 2014. *Computaional Fluid Dynamics (CFD) Analysis of Air Based Building Integrated Photovoltaic Thermal (BIPV/T) Systems for Efficient Performance.* Ottawa, s.n.

Guiavarch, A. & Peuportier, B., 2006. Photovoltailc Collectors Efficiency According to Their Integration in Buildings. *Solar Energy*, 1, pp. 65-77.

Incropera, F. P., DeWitt, D. P., Bergman, T. L. & Lavine, A. S., 2006. *Fundamentals of Heat and Mass Transfer.* 6th ed. New Jersey: John Wiley & Sons.

International Energy Agency (IEA), 2002. *Potential for Building Integrated Photovoltaics: Photovoltaic Power Systems Progremme,* Paris: International Energy Agency.

Jubayer, C. M., Karava, P. & Savory, E., 2010. *CFD Simulations for Evaluation of Forced Convective Heat Transfer Coefficient on Photovoltaic/Thermal Systems Integrated on the Windward Roof Surface of a Low-rise Building.* Chapel Hill, North Carolina, USA, s.n.

Karava, P., Jubayer, C. M., Savory, E. & Li, S., 2012. Effect of Incident Flow Conditions on Convective

Heat Transfer from the Inclined Windward Roof of a Low-rise Building with Application to Photovoltaic-thermal Systems. *Journal of Wind Engineering and Industrial Aerodynamics,* Volume 104-106, pp. 428-438.

King, D. L., Boyson, W. E. & Kratochvill, J. A., 2004. *Photovoltaic Array Performance Model,* Albuquerque: Sandia National Laboratories.

Kouyunbaba, B. K., Yilmaz, Z. & Ulgen, K., 2013. An Approach for Energy Modeling of a Building Integrated Photovoltaic (BIPV) Trombe Wall System. *Energy and Buildings,* Volume 67, pp. 680-688.

Krauter, S., 2004. Increased electrical yield via water flow over the front of photovoltaic panels. *Solar Energy Materials and Solar Cells,* 82(1-2), pp. 137-137.

Krawietz, S. A., 2011. *Sustainable Buildings and BIPV: an international perspective.* [Online] Available at: http://www.bre.co.uk/filelibrary/BIPV%202/Silke_Krawietz.pdf [Accessed 15 8 2015].

Launder, B. E. & Spalding, D. B., 1972. *Lectures in Mathemeatical Models of Turbulence.* London: Academic Press Inc..

Liao, L. et al., 2007. Numercial and Experimenatl Study of Heat Transfer in a BIPV-Thermal System. *Solar Energy Engineering,* 129(4), pp. 423-430.

Li, S. & Karava, P., 2012. Evaluation of Turbulence Models for Airflow and Heat Transfer Prediction in BIPV/T Systems Optimization. *Energy Procedia,* Volume 30, pp. 1025-1034.

McAdams, W. A., 1954. *Heat Trnasmission.* 3rd ed. New York: McGraw-Hill.

Mei, L., Infield, D., Eicker, U. & Fux, V., 2003. Thermal Modelling of a Building with an Integrated Ventilated PV Facade. *Energy and Buildings,* 35(6), pp. 605-617.

Mirzaei, P. A. & Carmeliet, J., 2013a. Dynamical Computational Fluid Dynamics Modelling of the Stochastic Wind for Application of Urban Studies. *Building and Environment,* Volume 70, pp. 161-170.

Mirzaei, P. A. & Carmeliet, J., 2013b. Influence of the Underneath Cavity on Buoyant-forced Cooling of the Integrated Photovoltaic Panels in Building Roff: A Thermography Study. *Progress in Photovoltaics: Research and Applications,* 23(1), pp. 19-29.

Mirzaei, P. A. & Haghihat, F., 2011. Pollution Removal Effectiveness of the Pedestrian Ventilation System. *Journal of Wind Engineering and Industrial Aerodynnamics,* 99(1), pp. 46-58.

Mirzaei, P. A., Paterna, E. & Carmeliet, J., 2014. Investigation of the Role of Cavity Airflow on the

Performance of Building-integrated Photovoltaic Panels. *Solar Energy,* Volume 107, pp. 510-522.

Mirzaei, P. A. & Rad, M., 2013. Toward Design and Fabrication of Wind-driven Vehicles: Procedure to Optimize the Threshold of Driving Forces. *Applied Mathematical Modelling,* 37(1-2), pp. 50-61.

Mirzaei, P. A. & Zhang, R., 2015. Validation of a Climatic CFD Model to Predict the Surface Temperature of Building Integrated Photovoltaics. *Energy Procedia,* Volume 78, pp. 1865-1870.

Onur, N., 1993. Forced Convection Heat Transfer From a Flat-plate Model Collector on Roof of a Model House. *Wärme and Stoffübertragung,* Volume 28, pp. 141-145.

Puleo, J. A., Mouraenko, O. & Hanes, D. M., 2004. One-dimensional Wave Bottom Boundary Lyaer Model Comparison: Specific Eddy Viscosity and Turbulence Closure Models. *Journal of Waterway Port Costal and Ocean Engineering,* 130(6), pp. 322-325.

Renewable Energy Policy Network for the 21st Century (REN21), 2014. *Renewables 2014 Global Status Report,* Paris: REN21 Secretariat.

Skoplaki, E. & Palyvos, J. A., 2009. Operating Temperature of Photovoltaic Modules: A Survey of pertinent correlations. *Renewable Energy,* 34(1), pp. 23-29.

Tominaga, Y. et al., 2008. AIJ Guidelines for Practical Applications of CFD to Pedestrian Wind Environment Around Buildings. *Journal of Wind Engineering and Industrial Aerodynamics,* 96(10-11), pp. 1749-1761.

Turgut, O. & Onur, N., 2009. Three Dimensional Numeridcal and Experimental Study of Forced Convection Heat Transfer on Solar Collector Surface. *International Communications in Heat and Mass Transfer,* Volume 36, pp. 274-279.

Wilson, M. J. & Paul, M. C., 2011. Effect of Mounting Geometry on Convection Occuring Under a Photovoltaic Panel and the Corresponding Effiiciency Using CFD. *Solar Energy,* 85(10), pp. 2540-2550.